VOL.40 Nº1 2023
https://doi.org/10.22491/rmct.v40i1.9484.en

Production and characterization of HA, HA/SiO_2, and KNN biomaterial granules

Pedro de Farias Vanzan[1], Suzana Noronha Ferreira Ribeiro[1], Amal Elzubair[1], Marcelo Henrique Prado da Silva*[1]
[1]Military Institute of Engineering (IME)
Praça General Tibúrcio, 80 – Urca, Rio de Janeiro (RJ), Brazil
***marceloprado@ime.eb.br**

ABSTRACT: *Repair and replacement of damaged or lost tissue is a problem of utmost importance for contemporary medicine. Hydroxyapatite,] (HA), is the bioceramic most similar to the inorganic phase of bone tissue, besides being bioactive. Hydroxyapatites with partial ionic substitutions and other bioactive bioceramics are adopted as synthetic bone grafts. These grafts can be produced in different forms, such as microspheres, porous scans, or granules. In this work, HA partially replaced with biogenic silica and sodium-potassium niobates (KNN) were synthesized and processed in the form of granules. The materials were calcined, pressed, sintered, ground and then sieved. The samples were characterized by X-ray diffraction (XRD), scanning electron microscopy (SEM) and energy dispersion spectroscopy (EDS). The results showed the presence of micrometric and manometric pores in the HA samples, with higher porosity in the samples with higher percentage of silica.*

KEYWORDS: *Hydroxyapatite. Piezoelectricity. Biomaterials. Granules.*

RESUMO: *O reparo e a substituição de tecido lesado ou perdido é um problema de extrema importância para a medicina contemporânea. A hidroxiapatita, $Ca_{10}(PO_4)_6(OH)_2$, (HA), é a biocerâmica mais similar à fase inorgânica do tecido ósseo, além de ser bioativa. Hidroxiapatitas com substituições iônicas parciais e outras biocerâmicas bioativas são adotadas como enxertos ósseos sintéticos. Estes podem ser produzidos em diferentes formas, tais como microesferas, arcabouços porosos ou grânulos. Neste trabalho, HA parcialmente substituída com sílica biogênica e niobato de sódio e potássio (KNN) foram sintetizados e processados sob a forma de grânulos. Os materiais foram calcinados, prensados e sinterizados, posteriormente sendo moídos e peneirados. As amostras foram caracterizadas por difração de raios X (DRX), microscopia eletrônica de varredura (MEV) e espectroscopia por dispersão de energia (EDS). Os resultados mostraram a presença de poros micrométricos e nanométricos nas amostras de HA, com maior porosidade naquelas com maior porcentagem da sílica.*

PALAVRAS-CHAVE: *Hidroxiapatita. Piezeletricidade. Biomateriais. Grânulos.*

1. Introduction

Biomaterials are biocompatible materials, either natural or synthetic, and can belong to any class, including metals, ceramics, polymers or composites. They must be capable of partially or completely replacing organs or functions of the human body. Metallic biomaterials are used in structural applications in which tensile, compressive, flexural and torsional strength are required. For example, orthopedic and dental implants are designed so that metals or metal alloys fulfill their function based on the application and the host site [1]. Non-structural metallic biomaterials include stents with a shape memory effect, which are flexible metallic structures inserted into the human body after being plastically deformed. When body temperature is reached, these stents return to their original shape [2].

Biocompatible ceramics, or bioceramics, are used in various applications. Inert types, or bioinerts, are employed when chemical inertness is a fundamental requirement. These materials are generally very hard and resistant to abrasion. Alumina (Al_2O_3) and zirconia (ZrO_2) are examples of bioinert bioceramics used in femoral head prostheses, where chemical inertness, abrasion resistance, and hardness are crucial [3]. On the other hand, bioactive bioceramics can chemically bond to bone. These are used as bioactive coatings on metallic implants, providing a chemical bonding interface between bone tissue and the metallic implant, which bioceramics alone would not fulfill [4].

Bioglasses, or biocompatible glasses, are often categorized with bioceramics since they are formed from both metallic and non-metallic elements. When subjected to thermal treatments, bioglasses can become partially ceramic, glass-ceramic, or even fully crystallized, forming bioceramics. Bioactive bioglasses can also be used as coatings for metal implants.

Among bioactive bioceramics, research on calcium phosphate-based materials has shown

promising results for bone defect repair. Bioactive bioceramics are used in trauma treatments for bone regeneration, healing, and reconstitution. Their biocompatibility is a direct result of their chemical composition. Hydroxyapatite ($Ca_{10}(PO_4)_6(OH)_2$) is the most commonly used bioceramic as a synthetic bone graft because it is bioactive, meaning it can chemically bind to bone. Additionally, ionic substitutions can alter its rate of bioreabsorption in biological media. The synthesis of hydroxyapatites with ionic substitutions is a well-studied area, as human bone is a composite material based on collagen and hydroxyapatite nanoparticles, with substitutions of ions such as Zn^{2+}, K^+, Mg^{2+}, and Na^+ [5].

Bioglasses added to hydroxyapatite (HA) during the sintering process result in glass-reinforced hydroxyapatites. If these bioglasses are silicatic, the silicon or silicate group can integrate into the hydroxyapatite structure [6,7]. Silicon dioxide or silica (SiO_2), in its amorphous form, has been used in medical and dental applications because the presence of silica contributes to bioactivity [8]. This is directly related to the material's ability to form bridges in the presence of silica in biological media [8].

Other considerations related to the sintering of glassreinforced hydroxyapatites involve the presence of liquid phase, the possibility of ionic substitutions during the process, and the decomposition of hydroxyapatite into more soluble phases *in vitro* and *in vivo*.

Sintering in the presence of a liquid phase is a key factor in producing hydroxyapatite composites reinforced with bioglass. The reinforcement results from the increased densification achieved by adding bioglass powder. When bioglass melts, it wets the hydroxyapatite particles, and capillary forces promote densification. Additionally, the presence of a liquid phase enhances diffusional mechanisms, as diffusion is much more effective in the liquid state than in the solid state. Since densification occurs through diffusional mechanisms that bring ceramic powder particles closer together, GR-HA (glass-reinforced hydroxyapatite) samples tend to be denser than HA (pure hydroxyapatite) samples pressed and sintered under the same conditions.

Sintering additives can interact with the primary ceramic powder in several ways: they may form a new phase, promote partial ionic substitutions in the main phase, or remain as a non-soluble second phase within the primary phase [9]. The hydroxyapatite structure allows for substitutions of both anionic and cationic groups. Thus, using bioglasses as sintering additives (or reinforcements) to hydroxyapatite powder is a strategy for synthesizing partially substituted hydroxyapatites [10]. Depending on the bioglass composition, cationic and/or anionic groups can cause partial or total substitutions in the HA structure [10].

The properties of hydroxyapatite, such as bioactivity, thermal stability, and bioresorption rate *in vivo* and *in vitro*, are directly related to its crystallinity and the presence of cationic and anionic substitutions in the crystal lattice [10]. Cationic and anionic substitutions affect hydroxyapatite crystallinity by creating defects in the lattice. Substitutions with F^- and $(CO_3)^{2-}$ ions have opposing effects on crystallinity: replacing $(OH)^-$ groups with F^- anions increases crystallinity, while substitutions of $(OH)^-$ groups with $(CO_3)^{2-}$ anions decrease it. This effect is also observed when $(CO_3)^{2-}$ groups replace $(PO_4)^{3-}$ groups [10]. This explains why fluorapatites are more crystalline than carbonate apatites.

Among the biologically relevant elements, silicon is notable for promoting biomineralization and playing a crucial role in bone metabolism [8, 11]. Silicon is therefore studied for partial substitution in the structure of hydroxyapatite and bioglasses. In hydroxyapatite, silicate groups $(SiO_4)^{4-}$ partially replace phosphate groups $(PO_4)^{3-}$. Many authors set a limit of 5% w/w of Si (approximately 1.7 mol Si/1 mol HA). Silicon additions introduce defects in the HA structure, leading to decomposition into phases such as tricalcium phosphate ($Ca_3(PO_4)_2$) after sintering [11].

The crystallinity of hydroxyapatite affects its properties, including bioactivity. More crystalline materials are less bioactive and have lower bioresorption rates *in vivo* and *in vitro*. For this reason, fluorapatites are less bioactive and have lower

bioresorption rates [12]. Thermal stability is also dependent on crystallinity: the more crystalline the HA, the more thermally stable it is. Therefore, sintering hydroxyapatites with varying degrees of crystallinity at the same temperature can yield different phases. Highly crystalline hydroxyapatites are more thermally stable, resulting in higher thermal decomposition temperatures. Conversely, substitutions that reduce crystallinity lower the thermal decomposition temperature. For example, sintering fluorapatite and carbonate apatite at the same temperature can produce highly crystalline fluorapatite as a single phase in the fluorapatite sample, and a mixture of hydroxyapatite and tricalcium phosphate in the carbonate apatite sample [13]. These effects illustrate that GR-HA composites can be more or less bioactive than pure HA and can exhibit different bioresorption rates *in vivo* and *in vitro*. They can consist of various phases such as HA, partially substituted HA, orthorhombic tricalcium phosphate (α-TCP), or rhombohedral tricalcium phosphate (β-TCP), among others [14]. Comparing hydroxyapatite with tricalcium phosphates, the order of bioresorption *in vivo* and *in vitro* is α-TCP > β-TCP > HA.

Ceramics based on biphasic calcium phosphates, containing HA + β-TCP, or three-phase ceramics, containing HA + α-TCP + β-TCP, are strategies for developing alloplastic (synthetic) bone grafts. Bone grafts can be autogenous (from the patient), allogenous (from donors of the same species), xenogenic (from animals of another species), or alloplastic/synthetic [15]. Alloplastic grafts have the advantage over allografts and xenografts of not being vectors for pathogen transmission. Autogenous grafts are considered the gold standard for bone repair because they carry growth factors from the donor. These grafts are osteoinductive, meaning they can induce differentiation of undifferentiated cells into osteoblasts. However, extensive lesions would require creating a large defect in the donor, which can result in morbidity [16]. The bioceramics most commonly used as alloplastic grafts include HA, biphasic calcium phosphate (HA + TCP), and bioglasses.

Fig. 1 - Bone regeneration with the help of HA-containing graft. Source [17]**.**

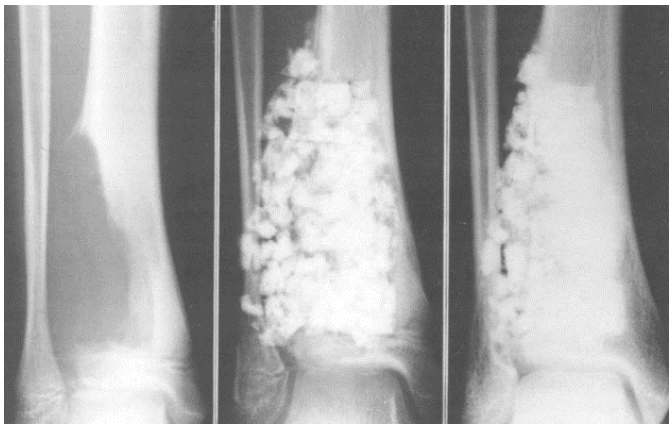

(a) (b) (c)

Figure 1 illustrates the use of an alloplastic graft in repairing a bone defect. It presents, in (a), a bone defect; in (b), the defect shortly after being filled with HA granules; and, in (c), the radiographic image of the defect immediately after surgery and three years later [17]. The latest generation of alloplastic grafts includes granules and porous scaffolds made from bioactive, bioresorbable, and preferably osteoinductive bioceramics. Recent studies highlight piezoelectric bioceramics as a new alternative to calcium phosphates and bioglasses [18]. *In vivo* studies suggest that applying direct current electrical stimulation to an implant site enhances early-stage implant osseointegration and interfacial resistance, and promotes bone tissue formation. Piezoelectric materials can mimic the bone's ability to generate electrical potentials under mechanical load without requiring an external energy source [18]. Bioactive and piezoelectric bioceramics, such as sodium niobates (KNN), (which are potassium) combine bioactivity and piezoelectricity, making KNN a promising candidate for alloplastic grafting [18].

In this study, pure hydroxyapatite granules (HA0), hydroxyapatite with biogenic silica (HA5 and HA10), and KNN were produced and characterized.

2. MATERIALS AND METHODS

The materials used in this study included: HA powders, silica (SiO_2), KNN powders calcined at different temperatures, and polyethylene wax beads (Licowax PE 830 from Clariant). The silica was sourced from the freshwater sponge *Metania reticulata*, collected in the Amazon region. The HA powders were mixed with 5% to 10% by weight of silica.

The hydroxyapatite (HA) was synthesized via precipitation in an aqueous medium from a precursor solution containing (Ca^{2+}) cations and (PO_4^{3-}) anions, with pH control at room temperature. The synthesis method is described by [19]. It involves aqueous reactions between phosphate and calcium precursors with controlled pH and temperature. A suspension of 0.5 M calcium hydroxide ($Ca(OH)_2$) was prepared under magnetic stirring. Simultaneously, a 1 M solution of lactic acid ($C_3H_6O_3$) was prepared and added to the calcium hydroxide suspension. Then, a 0.3 M solution of phosphoric acid (H_3PO_4) was prepared and slowly added to the mixture at a rate of 8 mL/min. The resulting solution, known as the precursor solution, was stirred for 24 hours. Sodium hydroxide (NaOH) was then added to adjust the pH to 12, allowing the precipitation of hydroxyapatite. The precipitate was aged for 24 hours without stirring, filtered using filter paper and a vacuum system, and resuspended in deionized water to remove excess NaOH, achieving a pH of 7. The precipitate was then dried in an oven at 60°C for 24 hours.

To incorporate silica into hydroxyapatite, a composite was produced using hydroxyapatite obtained by the precipitation method and silica from calcined freshwater sponge. Five different percentages of silica were used to create a ceramic slip composed of hydroxyapatite, biogenic silica, water, and polyethylene glycol (PEG). The resulting paste was applied to polymeric sponges, which served as a porous framework for the ceramic paste. The sponges were immersed in the paste for 12 hours, then heat-treated with a heating rate of 0.5°C/min up to 550°C, where they were held for 2 hours to remove PEG and other organic additives.

KNN was synthesized using the sol-gel method, chosen for its simplicity and the homogeneity of the final material, as described by Jigong et al. [8]. The raw materials included potassium carbonate (K_2CO_3), sodium carbonate (Na_2CO_3), niobium(V) oxide (NbO_5), and citric acid ($C_6H_8O_7{\cdot}H_2O$). The carbonates were dissolved in deionized water and stirred for 20 minutes. Citric acid was then added to the carbonate solution. An ammonia solution was added to adjust the pH and form the sol. Niobium(V) oxide was introduced into the sol, and the mixture was ground with alumina spheres for 8 hours. The resulting paste (Figure 3) was dried at 120°C to form xerogel, which was then calcined at 650°C, 700°C, and 750°C for 2 hours to obtain the powders.

The powders were mixed with polyethylene (PE) wax beads in a volumetric ratio of 65% (v/v) powder to 35% (v/v) wax beads. The mixture was pressed at 50 MPa for 1 minute. The green bodies of the samples were sintered with a heating ramp up to 550°C to eliminate the PE beads, with a heating rate of 0.5°C/min and a 2-hour hold at 550°C. Sintering continued at a rate of 3°C/min up to 1100°C, with a 1-hour hold at 1100°C. The sintered pellets were ground and sieved to granule sizes between 0.18 mm and 0.71 mm. Finally, the structure of the granules was characterized by X-ray diffraction (XRD) using an X'PERT PRO MRD diffractometer (PANalytical) with a cobalt-CoKα source (λ=1.789 Å), a current of 30 mA, and a voltage of 40 kV, scanning from 10° to 80° 2θ with a step size of 0.02 seconds. Qualitative phase analysis was performed using HighScore Plus software. The morphology and chemical composition of the granules were assessed using a Field Emission Gun Scanning Electron Microscope (FEG-SEM), model QUANTA 250 FEG from FEI, coupled with an energy dispersive spectrometer (EDS), model Bruker 6-60.

3. RESULTS AND DISCUSSION

3.1 XRD analysis

Figure 2.4 presents the results of the X-ray diffraction (XRD) analyses for hydroxyapatite (HA) samples, both pure and partially substituted with SiO_2, after sintering at 1100°C. The analysis revealed that the samples without biogenic silica addition exhibited a single phase of hydroxyapatite (HA). In contrast, the samples

containing 5% w/w and 10% w/w SiO_2 displayed additional phases of whitlockite ($Ca_3(PO_4)_2$) and silica (SiO_2). These findings demonstrate the effect of biogenic silica on the thermal stability of HA. Specifically, the addition of silica led to phase transformations upon sintering at 1100°C, whereas the pure HA samples retained a single phase of hydroxyapatite at the same temperature. This observation supports previous studies indicating that silica influences the phase stability of HA.

It was also observed that the HA phase showed less intense and wider peaks in the samples that received biogenic silica. This result corroborates the effect of ionic substitutions with $(SiO_4)^{4-}$ groups in the crystallinity of HA [11]. These authors report the creation of defects in the structure of HA, due to the substitutions of $(PO_4)^{3-}$ groups by $(SiO_4)^{4-}$ groups. In fact, [21] reported the creation of $(OH)^-$ group vacancies due to the need for load rebalancing, since there is a difference between the loads of the $(PO_4)^{3-}$ groups and $(SiO_4)^{4-}$ groups. The variation in ionic radii between these groups also induces stress in the HA lattice, contributing to the observed reduction in crystallinity in the samples with ionic substitutions.

Fig. 2 - X-ray diffractogram of HA samples with and without addition of biogenic silica.

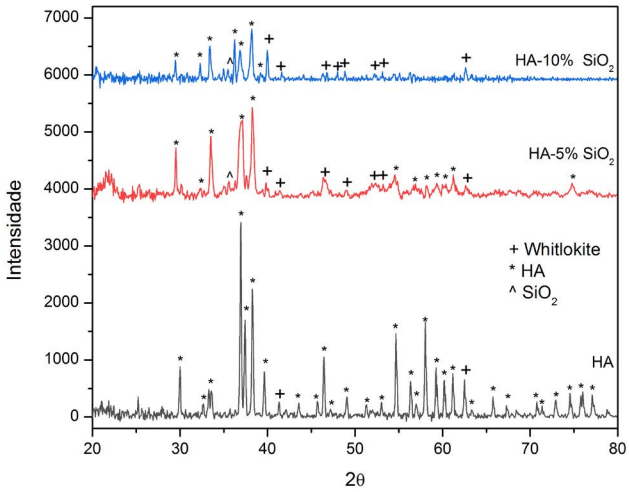

The XRD analysis of KNN samples, shown in Figures 3 to 5, identified three phases: $K_{0.5}Na_{0.5}NbO_3$, $K_6Nb_{10.8}O_{30}$ (KNN) and Al_2O_3, with KNN being the predominant phase. Some peaks corresponding to alumina (Al_2O_3) were also observed, likely due to the grinding process during synthesis.

Fig. 3 - X-ray diffractograms of KNN samples.

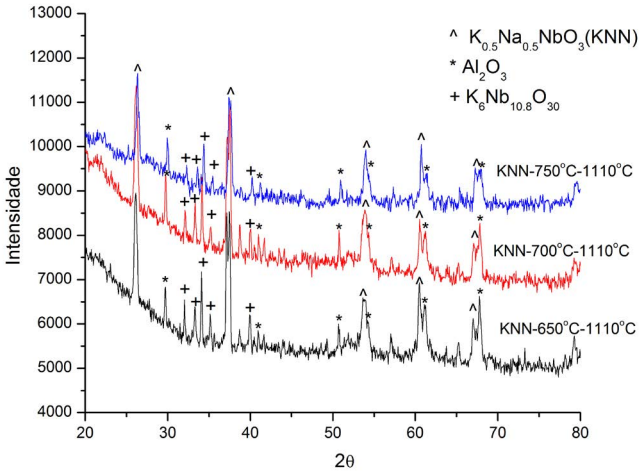

3.2 SEM analysis

Figures 4 to 9 present the scanning electron microscopy with field emission gun (SEM-FEG) analysis of the HA samples. These images confirm that the granule sizes fall within the predicted range. Notably, an increase in porosity is observed with higher percentages of silica, as illustrated in Figures 7 to 9.

Fig. 4 - SEM micrograph of the HA0 sample at 100× magnification.

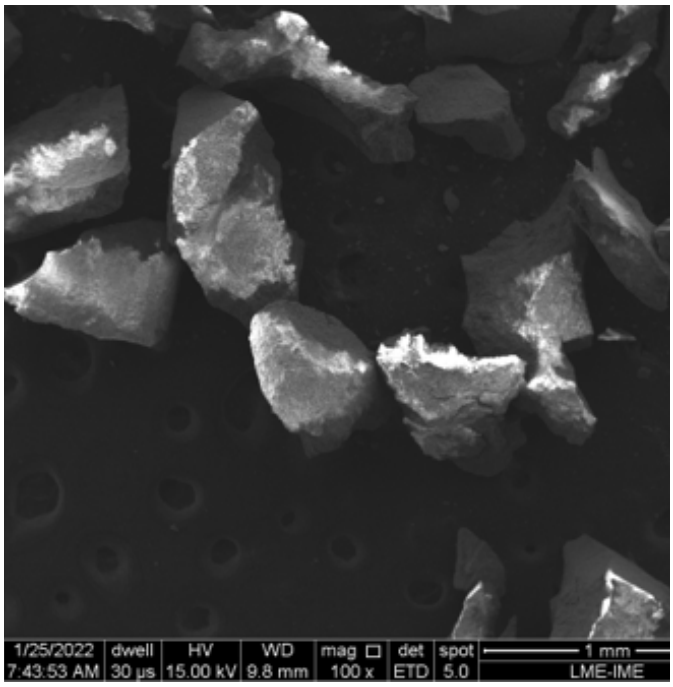

Fig. 5 - SEM micrograph of the HA5 sample at 100× magnification.

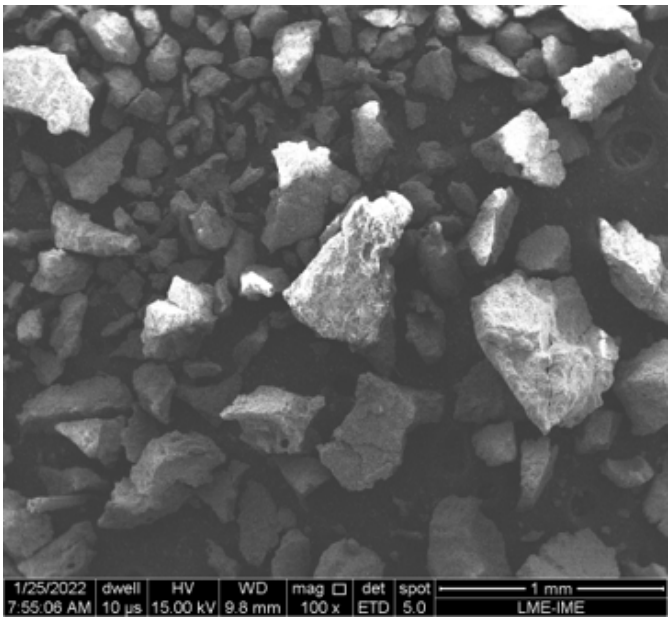

Fig. 6 - SEM micrograph of the HA10 sample at 100× magnification.

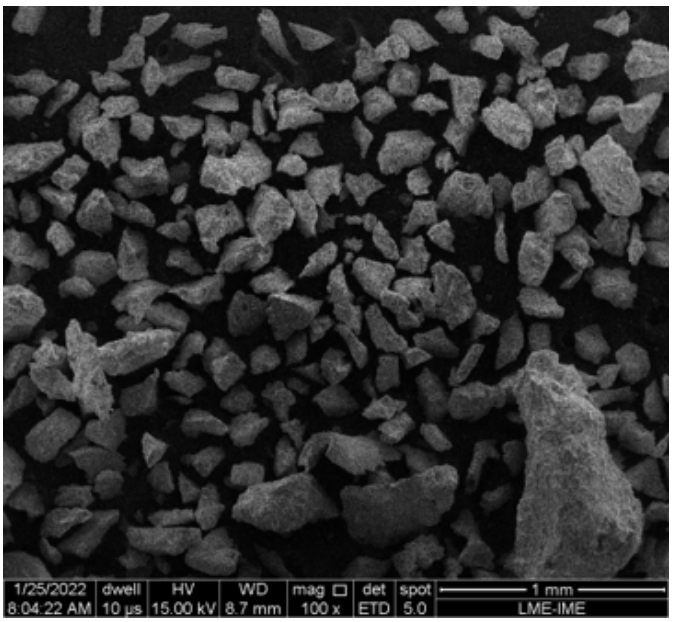

Fig. 7 - SEM micrograph of the HA0 sample at 5000× magnification

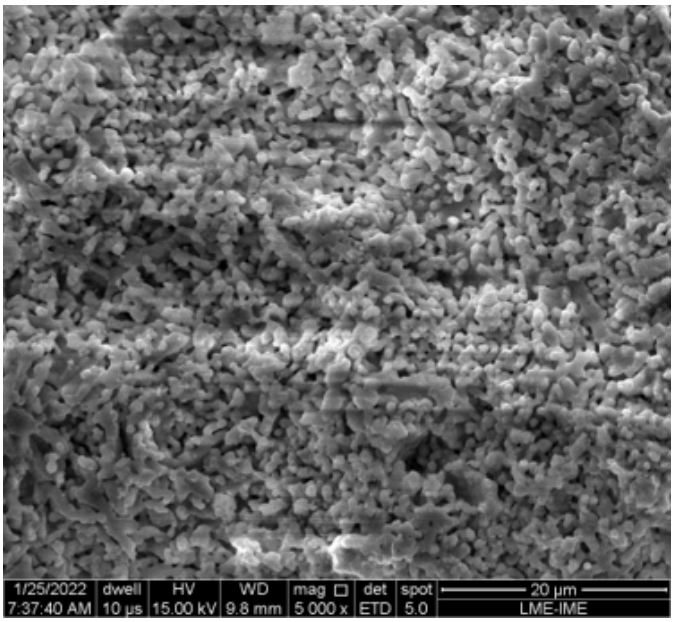

Fig. 8 - SEM micrograph of the HA5 sample at 5000× magnification.

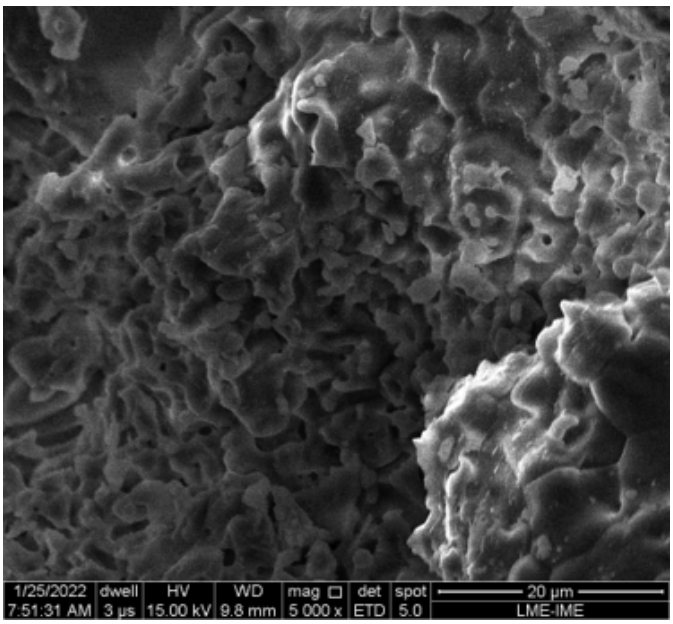

Fig. 9 - SEM micrograph of the HA10 sample at 5000× magnification.

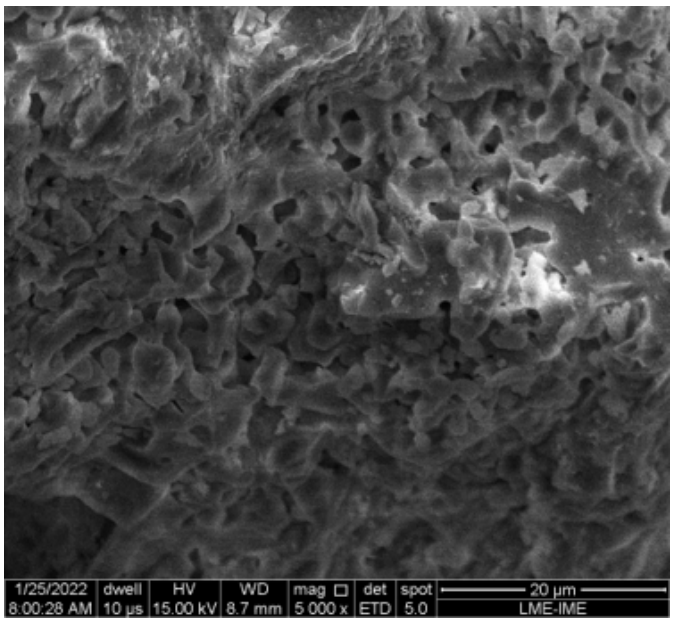

Fig. 10 - SEM micrograph of the KNN650 sample at 100× magnification.

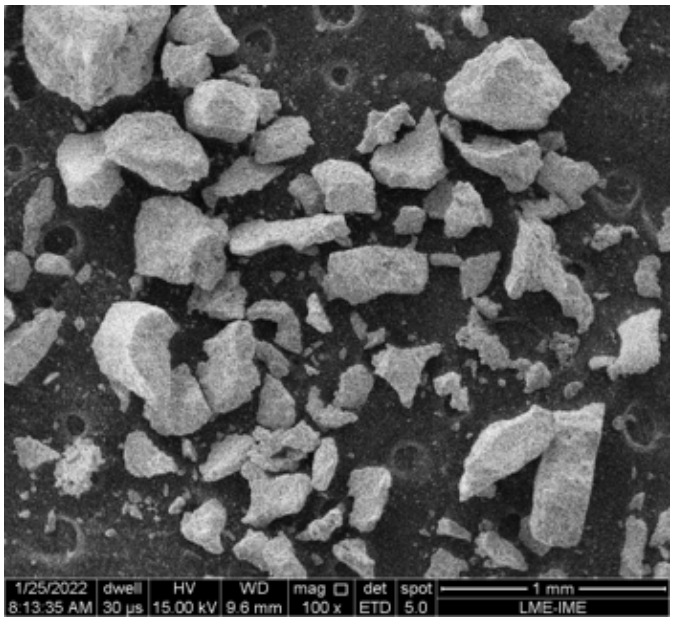

The results of SEM analysis of KNN samples are presented in Figures 10 to 15. Figures 10 to 12 also confirmed the particle size range, in accordance with the sieving process. Figures 12 to 15 revealed changes in the morphologies of the granules, with an increase in the calcination temperature.

Fig. 11 - SEM micrograph of the KNN700 sample at 100× magnification.

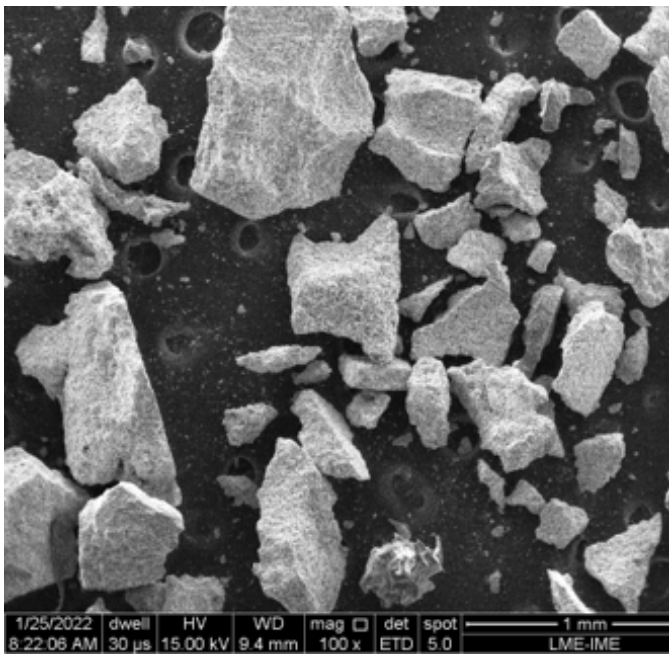

Fig. 12 - SEM micrograph of the KNN750 sample at 100× magnification.

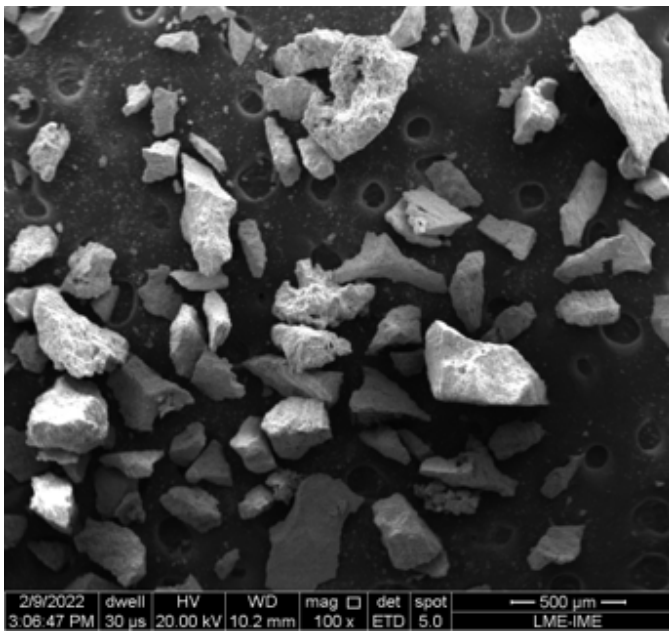

Fig. 13 - SEM micrograph of the KNN650 sample at 5000× magnification.

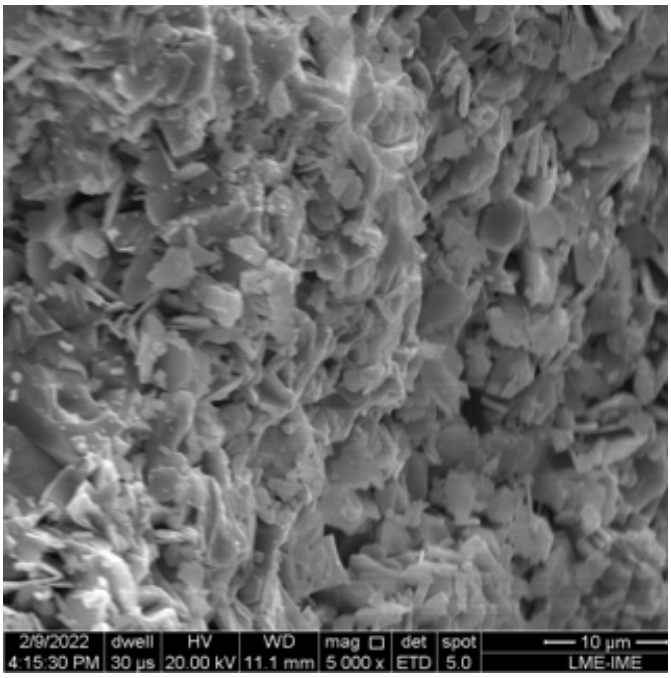

Fig. 14 - SEM micrograph of the KNN700 sample at 5000× magnification.

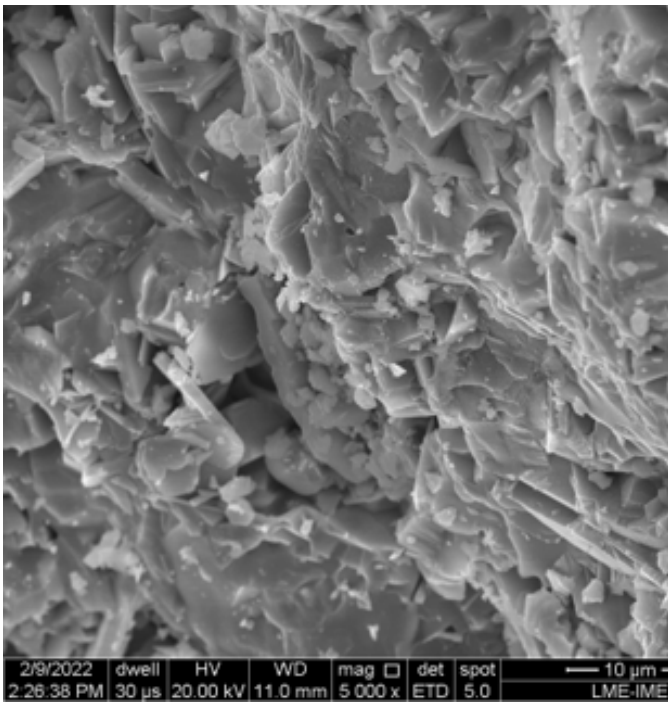

Fig. 15 - SEM micrograph of the KNN750 sample at 5000× magnification.

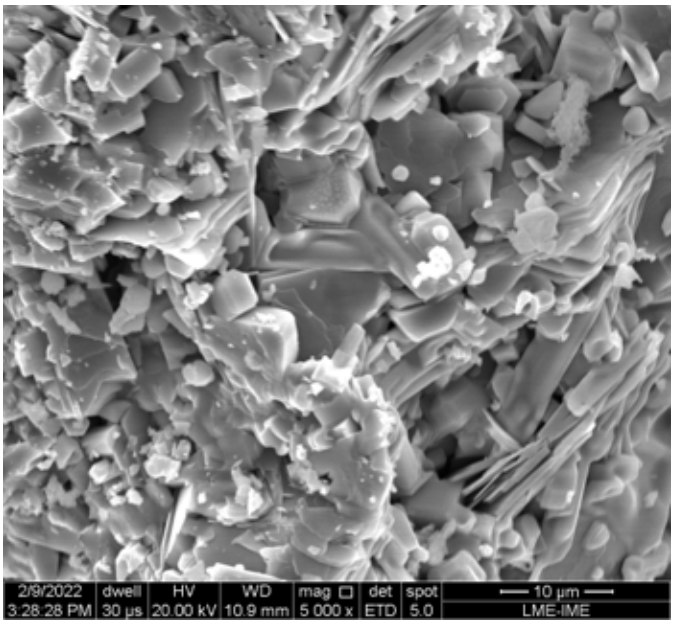

3.2 EDS analysis

The energy-dispersive X-ray spectroscopy (EDS) analysis of the HA samples confirmed the presence of calcium (Ca), phosphorus (P), and oxygen (O), as shown in the spectrum in Figure 16. The table included in this figure provides atomic and weight fractions. It is important to note that EDS is a semiquantitative technique, which means the results should be considered with this limitation in mind. Nonetheless, the EDS results are consistent with those obtained from the XRD analysis of the HA samples.

For HA samples with added biogenic silica, the EDS analysis revealed the presence of calcium (Ca), phosphorus (P), oxygen (O), and silicon (Si), as illustrated in Figures 17 and 18. These findings support the XRD results, which indicated the presence of the SiO_2 phase in these samples.

In the KNN samples, EDS analysis detected the presence of potassium (K), sodium (Na), niobium (Nb), oxygen (O), and aluminum (Al), as shown in Figure 19. This corroborates the XRD results, which identified the Al_2O_3 phase in the samples. The presence of aluminum (Al) and oxygen (O) in the EDS spectra further confirms this phase.

Fig. 16 - EDS spectrum of the HA0 sample.

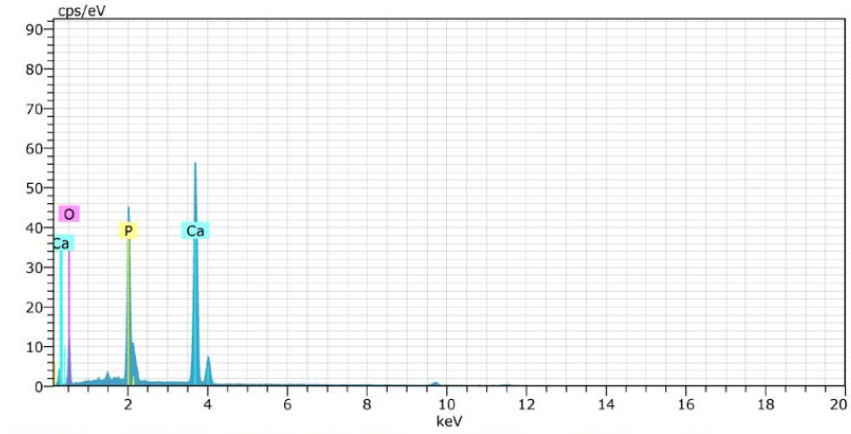

Area 84 Date:2/16/2022 12:05:44 AM HV:20.0kV Puls th.:23.00kcps

El	AN	Series	unn. C [wt.%]	norm. C [wt.%]	Atom. C [at.%]	Error (1 Sigma) [wt.%]
Ca	20	K-series	36.56	53.83	36.70	1.10
O	8	K-series	18.56	27.32	46.66	2.67
P	15	K-series	12.81	18.85	16.63	0.53
		Total:	67.92	100.00	100.00	

Fig. 17 - EDS spectrum of the HA5 sample.

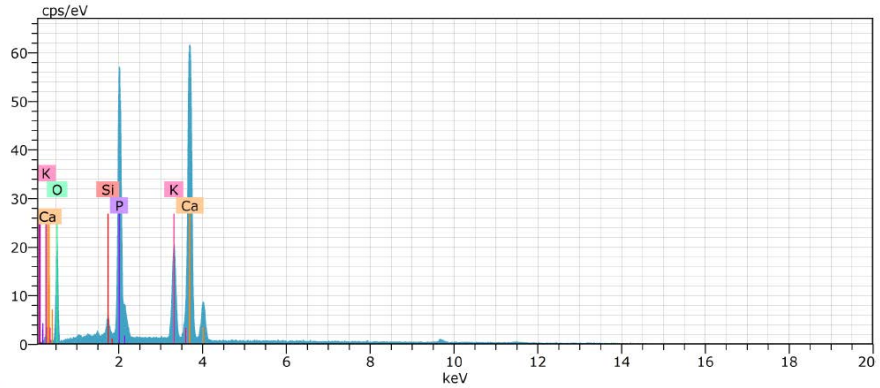

Area 5Date:1/25/2022 8:51:38 PM HV:20.0kV Puls th.:29.55kcps

El	AN	Series	unn. C [wt.%]	norm. C [wt.%]	Atom. C [at.%]	Error (1 Sigma) [wt.%]
Ca	20	K-series	28.44	43.58	29.12	0.86
O	8	K-series	19.16	29.35	49.14	2.68
P	15	K-series	11.07	16.95	14.66	0.46
K	19	K-series	6.22	9.54	6.53	0.22
Si	14	K-series	0.38	0.58	0.55	0.04
		Total:	65.27	100.00	100.00	

Fig. 18 - EDS spectrum of the HA10 sample.

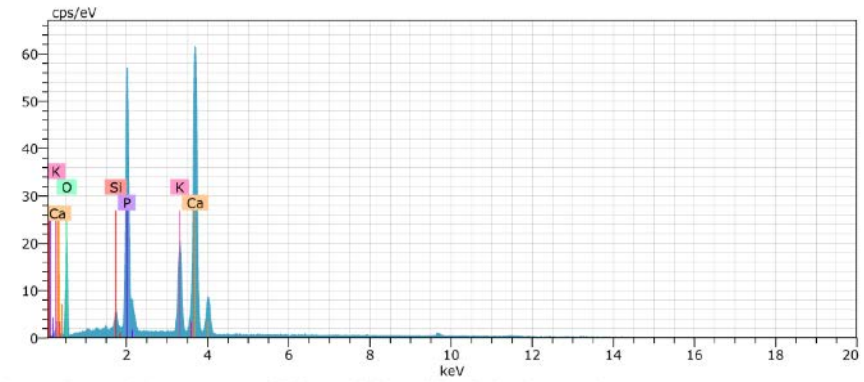

Area 5Date:1/25/2022 8:51:38 PM HV:20.0kV Puls th.:29.55kcps

El	AN	Series	unn. C [wt.%]	norm. C [wt.%]	Atom. C [at.%]	Error (1 Sigma) [wt.%]
Ca	20	K-series	28.44	43.58	29.12	0.86
O	8	K-series	19.16	29.35	49.14	2.68
P	15	K-series	11.07	16.95	14.66	0.46
K	19	K-series	6.22	9.54	6.53	0.22
Si	14	K-series	0.38	0.58	0.55	0.04
		Total:	65.27	100.00	100.00	

Fig. 19 - EDS spectrum of the KNN650 sample.

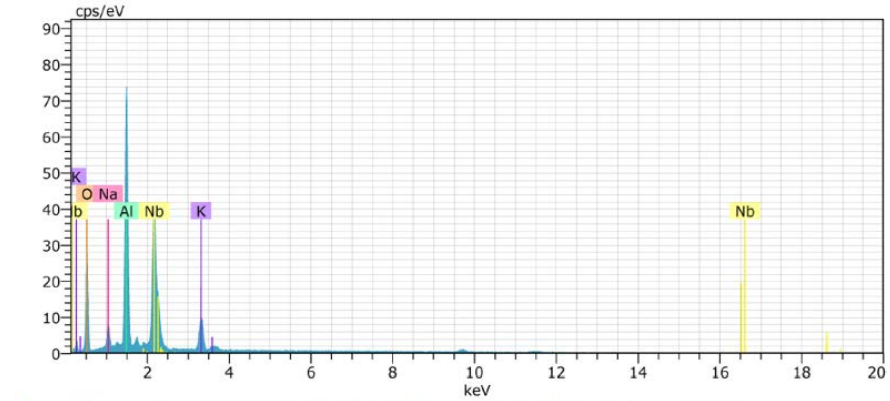

Area 83 Date:2/15/2022 11:59:29 PM HV:20.0kV Puls th.:25.84kcps

El	AN	Series	unn. C [wt.%]	norm. C [wt.%]	Atom. C [at.%]	Error (1 Sigma) [wt.%]
Nb	41	L-series	21.74	37.04	11.58	0.83
O	8	K-series	17.82	30.37	55.13	2.37
Al	13	K-series	13.99	23.84	25.66	0.70
K	19	K-series	3.85	6.57	4.88	0.15
Na	11	K-series	1.28	2.18	2.75	0.11
		Total:	58.68	100.00	100.00	

4. Conclusions

When comparing the HA granules, an increase in porosity was observed with higher silica content. This increased porosity enhances the specific surface area, which is beneficial for graft applications, as it boosts the bioactivity of the material and facilitates the permeation of body fluids. For the KNN granules, analysis revealed that no phase transformations occurred at the various calcination temperatures. After sintering at 1100ºC, the samples consistently exhibited three phases: $K_{0.5}Na_{0.5}NbO_3$, $K_6Nb_{10.8}O_{30}$ (KNN), and Al_2O_3. The presence of alumina is attributed to the milling process. The observed low density and alumina contamination could potentially impact the piezoelectric properties of the KNN granules, suggesting that the processing route may need further optimization.

Acknowledgements

This work was supported by the National Council for Scientific and Technological Development (CNPq), the Brazilian Metallurgy and Mining Company (CBMM), and the Coordination for the Improvement of Higher Education Personnel (CAPES).

References

[1] GORIAINOV, V.; COOK, R.; LATHAM, J. M.; DUNLOP, D. G.; OREFFO, R. O. C. Bone and metal: An orthopaedic perspective on osseointegration of metals. Acta Biomaterialia, v. 10, n. 10, p. 4043-4057, 2014.
[2] MAY, A.; SELMAIER, M.; HOCHBERGER, J.; GOSSNER, L.; MÜHLDORFER, S. HAHN, E. G., ELL, C. Memory metal stents for palliation of malignant obstruction of the oesophagus and cardia. Gut, v. 37, n. 3, p. 309-313, 1995.
[3] ALVES, H. L. R., STAINER, D., BERGMANN, C. P. Método alternativo para fabricação de cabeça femoral cerâmica para próteses de quadril. Revista Brasileira de Engenharia Biomédica, v. 20, n. 2-3, p. 81-88, 2004.
[4] RIGO, E. C. D. S.; OLIVEIRA, L. C.; SANTOS, L. A.; BOSCHI, A. O.; CARRODEGUAS, R. G. Implantes metálicos recobertos com hidroxiapatita. Revista Brasileira de Engenharia Biomédica, v. 15, n. 1-2, p. 21-29, 1999.
[5] HENCH, L. L. Biomaterials: a forecast for the future. Biomaterials, v. 19, n. 16, p. 1419-1423, 1998.
[6] FARZADI, A.; SOLATI-HASHJIN, M.; BAKHSHI, F. Synthesis and characterization of hydroxyapatite/β-tricalcium phosphate nanocomposites using microwave irradiation. Ceramics Internacional, v. 37, n. 1, p. 65-71, 2011.
[7] PUPIO, F. SANTOS, R.B.M., CAMARGO, N.H.A., DELIMA, S.A., GEMELLI, E. Síntese e caracterização de pós nanocompósitos fosfato de cálcio/SiO2n para aplicações biomédicas. In: Congresso Latino Americano de Órgãos Artificiais e Biomateriais, 5., 2008, Ouro Preto: COLAOB', 2008. v. 1, p. 1-6.
[8] BELLINI, O. J. Síntese e caracterização de uma matriz óssea de fosfato de cálcio e nanocompósitos de fosfato de cálcio/SiO2n para substituição e regeneração óssea. Dissertação (Mestrado) – Universidade Federal de Santa Catarina, Florianópolis, 2007.
[9] GERMAN, R. M.; RABIN, B. H. Enhanced Sintering Through Second Phase Additions. Powder Metallurgy, v. 28, n. 1, p. 7-12, 1985.
[10] ROCHA, D. N.; SILVA, M. H. P.; GOBBO, L. A. Produção de hidroxiapatita parcialmente substituída com nióbio. Revista Militar de Ciência e Tecnologia, p. 11-17, 2012.
[11] SZURKOWSKA, K.; KOLMAS, J. Hydroxyapatites enriched in silicon–Bioceramic materials for biomedical and pharmaceutical applications Progress in Natural Science: Materials International, v. 27, n. 4, p. 401-409, 2017.
[12] CHENG, K.; WENG, W.; QU, H.; DU, P.; SHEN, G.; HAN, G. et al. Sol-gel preparation and in vitro test of fluorapatite/hydroxyapatite films. Journal of Biomedical Materials Research, v. 69B, n. 1, p. 33-37, 2004.
[13] DJOUALLAH, S.; BELHOUCHET, H., KENZOUR, A.; KHERIFI, D. Sintering behavior of fluorapatite--based composites produced from natural phosphate and alumina. Ceramics International, v. 47, n. 3, p. 3553-3564, 2021.
[14] DUCHEYNE, P.; RADIN, S.; KING. L. The effect of calcium phosphate ceramic composition and structure on in vitro behavior. I. Dissolution. Journal of Biomedical Materials Research, v. 27, n. 1, p. 25-34, 1993.

[15] GIRÒN BASTIDAS, J.; BALDIN, E. K. K.; GODOI, T. P. M.; OLIVEIRA, L. S. D.; MACHADO, G. M.; MALFATTI, C. D. F.; PRANKE, P. H. L. Biomaterials for bone regeneration: an orthopedic and dentistry overview. Brazilian Journal of Medical and Biological Research, v. 54, n. 9, 2021
[16] BAUER, T. W.; MUSCHLER, G. F. Bone graft materials. An overview of the basic science. Clinical Orthopaedics and Related Research, v. 371, p 10-27.
[17] OONISHI, H. Orthopaedic applications of hydroxyapatite. Biomaterials, v. 12, n. 2, p. 171-178, 1991.
[18] POON, K. K.; WURM, M. C.; EVANS, D. M.; EINARSRUD, M. A.; LUTZ, R.; GLAUM, J. Biocompatibility of (Ba,Ca)(Zr,Ti)O_3 piezoelectric ceramics for bone replacement materials. Journal of Biomedical Materials Research, v. 108B, p. 1295-1303.
[19] PRADO DA SILVA, M. H., NAVARRO DA ROCHA, D. BR n PI 020110137091, 2011.
[20] JIGONG, H.; ZHIJUN, X. U.; RUIQING, C.; YANJIE, Z.; QIAN, C.; PENG, F. et al. Characterization of ($K_{0.5}Na_{0.5}$) NbO_3 powders and ceramics prepared by a novel hybrid method of sol–gel and ultrasonic atomization. Materials and Design, v. 31, n. 6, p. 3146–3150, 2010.
[21] GIBSON, I. R.; BEST, S. M.; BONFIELD, W. Chemical characterization of silicon-substituted hydroxyapatite. Journal of Biomedical Materials Research, v. 44, p. 422-428, 1999.